Electronic Supplementary Material (ESI) for Nanoscale.

Supporting Information for

Ru Nanoparticles Dispersed on Magnetic Yolk-Shell Nanoarchitectures with Fe_3O_4 Core and Sulfoacid-Containing Periodic Mesoporous Organosilica Shell as Bifunctional Catalysts for Direct Conversion of Cellulose to Isosorbide

Ying Yang*, Wen Zhang, Feng Yang, Biao Zhou, Dehong Zeng, Na Zhang, Guoming Zhao, Shijie Hao and Xin Zhang*

Email: catalyticscience@163.com

1. Experimental Section

1.1. Materials

Anhydrous $FeCl_3$, sodium citrate ($Na_3C_6H_5O_7$), sodium acetate (CH_3COONa), ruthenium chloride ($RuCl_3$), ascorbic acid ($C_6H_8O_6$), cetyltrimethyl ammonium bromide (CTAB), tetraethyl orthosilicate (TEOS), 1,4-bis(triethoxysilyl)ethane (BTEE, 92%), 3-mercaptopropyl trimethoxysilane (MPTMS), hydrogen peroxide (H_2O_2), sodium hydroxide, ammonia (25 wt%), ethylene glycol, and ethanol are of analytical grade, and were purchased from Sinopharm Chemical Reagent Co. Limited and used without any further purification. Microcrystalline cellulose was purchased from Alfa Aesar and used as received without any pretreatment. Standards (analytic grade) including sorbitol (Sinopharm Chemical Reagent Co. Ltd), erythritol and xylitol (Aladdin), 1,4-sorbitan (J&K), 1,5-sorbitan (Sigma-Aldrich), 2,5-sorbitan (Tronto Research Chemicals Inc.), isosorbide (Alfa Aesar), and ethylene glycol were directly used as received. Deionized water was used for all experiments.

1.2. Synthesis

1.2.1. Synthesis of Fe_3O_4 NPs

The water dispersible Fe_3O_4 particles were synthesized according to the method reported previously with slight modification.[1] Briefly, $FeCl_3$ (0.65 g, 4mmol), sodium citrate (0.20 g, 0.07 mmol), and sodium acetate (NaAc) (1.20 g, 14.6 mmol) were dissolved in ethylene glycol (20 mL) with magnetic stirring. The obtained yellow suspension was then transferred and sealed into a Teflon-lined stainless-steel autoclave (50 mL in capacity). The autoclave was heated at 200 ℃ for 10 h, and then allowed to cool to room temperature. The black products were washed with ethanol and deionized water 3 times, respectively.

1.2.2. Synthesis of Fe_3O_4@SiO_2

The $Fe_3O_4@SiO_2$ nanospheres were prepared through a versatile solution sol-gel method as follows. An aqueous dispersion of the magnetite particles (70 mL, 0.02 g mL^{-1}) was added to a three-neck round-bottom flask charged with absolute ethanol (200 mL) and concentrated ammonia solution (5.0 mL, 28 wt %) under mechanical stirring at 30 ℃ for 15 min. Afterward, 4.0 mL of TEOS was added dropwise in 2 min, and the reaction was allowed to proceed for 8 h under continuous mechanical stirring.

1.2.3. Synthesis of $Fe_3O_4@void@PMO\text{-}SH^n$

First, the core-shell-shell $Fe_3O_4@SiO_2@asPMO\text{-}SH$ was prepared *via* coating SH-functionalized PMO layer on $Fe_3O_4@SiO_2$, using CTAB-directed assembly of MPTMS and BTEE under alkaline conditions. Typically, 0.15 g of CTAB was dissolved in 30 mL of deionized water and stirred for 30 min, followed by addition of 18 mL of $Fe_3O_4@SiO_2$ colloidal suspension. After further stirring for 2 h, 0.15 g of CTAB combined with 0.35 mL of NaOH (2 M) was added and the resulting mixture was heated to 80 ^oC. Then a certain amount of MPTMS (x μL) and BTEE (170-x μL) was added at this temperature and further stirred for 24 h, where x was set to be 0, 13, 24, 39, 56, 73 and 85. The resulting gel was then filtered off and dried at 50 ^oC, yielding $Fe_3O_4@SiO_2@asPMO\text{-}SH^n$, where n represents the Si molar percentage of 3-MPTMS in total silicas (*i.e.* the feed ratio of MPTMS), corresponding to be 0.00, 0.08, 0.14, 0.23, 0.33, 0.43 and 0.50. The CTAB was removed by pyrolysis of $Fe_3O_4@SiO_2@asPMO\text{-}SH^n$ in N_2 atmosphere at 250 ^oC for 8 h. The resulting $Fe_3O_4@SiO_2@PMO\text{-}SH^n$ (0.5 g) was mixed with 15 mL $NH_3 \cdot H_2O$ and 25 mL of ethanol, and stirred at 60 ^oC for 24 h to remove the middle silica layer, affording $Fe_3O_4@void@PMO\text{-}SH^n$.

1.2.4. Synthesis of $Ru^d/Fe_3O_4@void@PMO\text{-}SO_3H^n$

1.2.4.1 Oxidation

Typically, 0.5 g of Fe_3O_4@void@PMO-SH^n was dispersed in 20 mL of ethanol and stirred for 10 min. Then 20 mL of H_2O_2 was added to the above mixture and further stirred at room temperature for 24 h. The resulting mixture was filtered and washed using ethanol, yielding Fe_3O_4@void@PMO-SO_3H^n.

1.2.4.2. Preparation of colloidal Ru NPs with different sizes

Colloidal Ru NPs with different size was prepared according to the literature method with some modifications.[2] Colloidal Ru NPs with a mean size of 0.9 and 2.2 nm were prepared through the reduction of aqueous solution of $RuCl_3$ (2.2 mM, 20 mL) using ascorbic acid (0.25 g) in a flask at 80 ^oC for 1 and 5 min, respectively. Colloidal Ru NPs (5.5 nm) were prepared by the reduction of $RuCl_3$ (2.2 mM) in 20 mL of ethylene glycol with ascorbic acid (0.25 g) in an autoclave at 180 ^oC for 40 min. Colloidal Ru (8.8 nm) NPs were produced by reduction of $RuCl_3$ (2.2 mM) with ascorbic acid (0.25 g) in ethylene glycol (20 mL) with refluxing at 180 ^oC for 12 h.

1.2.4.3. Impregnation of Ru NPs

First, 0.3 g of Fe_3O_4@void@PMO-$SO_3H^{0.14}$ was mixed with 20 mL of Ru NP suspension. The resulting mixture was stirred at room temperature for 24 h, and then filtered and washed using ethanol, yielding $Ru^{0.9}$/Fe_3O_4@void@PMO-$SO_3H^{0.14}$, $Ru^{2.2}$/Fe_3O_4@void@PMO-$SO_3H^{0.14}$, $Ru^{5.5}$/Fe_3O_4@void@PMO-$SO_3H^{0.14}$ and $Ru^{8.8}$/Fe_3O_4@void@PMO-$SO_3H^{0.14}$. Then Fe_3O_4@void@PMO-SO_3H^n was used as the starting material to immobilize Ru NPs (2.2 nm) as the same method, affording $Ru^{2.2}$/Fe_3O_4@void@PMO-$SO_3H^{0.00}$, $Ru^{2.2}$/Fe_3O_4@void@PMO-$SO_3H^{0.08}$, $Ru^{2.2}$/Fe_3O_4@void@PMO-$SO_3H^{0.14}$, $Ru^{2.2}$/Fe_3O_4@void@PMO-$SO_3H^{0.23}$,

$Ru^{2.2}/Fe_3O_4$@void@PMO-$SO_3H^{0.33}$, $Ru^{2.2}/Fe_3O_4$@void@PMO-$SO_3H^{0.43}$ and $Ru^{2.2}/Fe_3O_4$@void@PMO-$SO_3H^{0.50}$.

1.2.5. Synthesis of $Ru^{2.2}/Fe_3O_4$@SiO_2@PMO-$SO_3H^{0.43}$

First, pyrolysis of 1.25 g Fe_3O_4@SiO_2@asPMO-$SH^{0.43}$ was performed in N_2 atmosphere at 250 ^oC for 8 h, yielding Fe_3O_4@SiO_2@PMO-$SH^{0.43}$. Then 0.5 g of Fe_3O_4@SiO_2@PMO-$SH^{0.43}$ was dispersed in 20 mL of ethanol and stirred for 10 min. 20 mL of H_2O_2 was added to the above mixture and further stirred at room temperature for 24 h. The resulting mixture was filtered and washed using ethanol, yielding Fe_3O_4@SiO_2@PMO-$SO_3H^{0.43}$. Last, 0.3 g of Fe_3O_4@SiO_2@PMO-$SO_3H^{0.43}$ was mixed with 20 mL of Ru NP sol (2.2 nm). The resulting mixture was stirred at room temperature at 24 h, and then filtered and washed using ethanol, yielding $Ru^{2.2}/Fe_3O_4$@SiO_2@PMO-$SO_3H^{0.43}$.

1.3. Characterization

Transmission electron microscope (TEM) measurements were carried out on a JEOL JEM-2100 transmission electron microscope with a tungsten filament at an accelerating voltage of 200 kV. High-angle annular dark-field scanning TEM (HADDF-STEM), and energy dispersive X-ray (EDX) analyses were performed using a FEI Tecnai G2 F20 transmission electron microscope operated at a voltage of 200 kV. The samples were prepared by placing a drop of the prepared solution on the surface of a copper grid. The histograms of particle were established from the measurement of 100~200 particles. The average diameter d was calculated from the following formula:

$$d = \frac{\sum n_i d_i}{\sum n_i}$$

Powder X-ray diffraction (XRD) was conducted using D8 Advance (Bruker) diffractometer. Diffractogrames were recorded in reflection mode using Ni-filtered CuKα radiation (λ = 0.15406 nm). The samples were scanned in the ranges (2θ): 1.2 to 10^o and 5 to 80^o, at the scanning speed of 1^o min^{-1} and 4^o min^{-1}, respectively. N_2 adsorption/desorption isotherms were recorded at 77 K using a JW-BK222 static volumetric gas adsorption instrument manufactured by Beijing JWCB Sci. & Tech. Co., Ltd. Before measurements, the samples were de-gassed at 300 ^oC for 3 h in vacuum. Specific surface area was determined by the Brunauer-Emmett-Teller (BET) method and mesopore size distributions were measured using Barrett-Joyner-Halenda (BJH) method from the desorption branch of the isotherms. The linearized BET model was used to fit the microporous data within the relative pressure range of 0.001 < P/P_0 < 0.05. The micropore size distributions were determined using the Horvath-Kawazoe (H-K) method assuming slit pore geometry. The infrared spectra of samples were recorded in KBr disks using a Nicolet Nexus 870 FTIR spectrometer. X-ray photoelectron spectroscopy (XPS) was performed on a Thermo ESCALAB 250Xi X-ray photoelectron spectrometer (employing a monochromated Al-Kα) X-ray source (hν = 1486.6 eV). All of the binding energy peaks of XPS spectra were calibrated by placing the principal C1s binding energy peak at 284.8 eV. Peaks from all the high resolution core spectra were fitted with XPSPEAK 4.1 software, using mixed Gaussian-Lorentzian functions. The S content was determined by a KZDL-8A sulfur element analyzer (Zhengli Instruments Co. Ltd., China). TG analysis was carried out on NETZSCH STA 409 PC instrument from ambient temperature to 800 ^oC under N_2 atmosphere with a heating rate of 10 ^oC/min.

NH_3-TPD was performed by using a BEL-CAT-B-82 (Bel) instrument connected to a thermal conductivity detector. Typically, the sample loaded in a quartz reactor

was first pretreated with high-purity Ar at 500 ^{o}C for 1.0 h. After the sample was cooled to 100 ^{o}C, NH_3 adsorption was performed by switching the Ar flow to a NH_3-N_2 (5 vol% NH_3) gas mixture and then maintaining the temperature for 1.0 h. Then, the gas phase or the weakly adsorbed NH_3 was purged by high-purity Ar at the same temperature. NH_3-TPD was performed in the Ar flow by raising the temperature to 600 ^{o}C at a rate of 10 ^{o} min^{-1}, and the desorbed NH_3 molecules were detected by using an on-line thermal conductivity detector.

The $Ru^{2.2}/Fe_3O_4$@void@PMO-SO_3H^n acidity capacity of anchored sulfoacid groups were evaluated by a titration of the samples against a 0.05 M NaOH solution (previously standardised by titration with potassium hydrogenphthalate) in the presence of 1 M NaCl.

Ru content was estimated by inductively coupled plasma-atomic emission spectroscopy (ICP-AES) analysis conducted on a Perkin Elmer emission spectrometer. Certain amount of vacuum-dried $Ru^{2.2}/Fe_3O_4$@PMO-SO_3H^n was placed in a digester with PTFE lined, and dissolved in 4 mL of aqua fortis solution mixed with 1 mL of HF. Microwave digestion was carried out at 120 ^{o}C for 30 min to completely dissolve the metal species. After cooling, each solution was filtered through a 0.45 μm polyethersulfone filter and then submitted for analysis.

1.4. Conversion of cellulose.

Catalytic conversion of cellulose was carried out in a stainless-steel autoclave (Parr Instrument Company, 100 mL) typically at 6.0 MPa H_2 pressure. For each reaction, 0.60 g cellulose, 0.06 g catalyst and 30 mL water were put into the reactor. The sealed autoclave was charged and deflated with N_2 three times before it was pressurized with H_2 to 6.0 MPa at room temperature, and then heated at 180~245 ^{o}C stirred at rate of 500 r min^{-1} for a certain duration. After the reaction was finished, the catalyst was

quickly separated from the suspension using a NdFeB magnet, rinsed with water and re-dispersed into the mixture of new reactants to initiate another reaction. The resulting mixture was centrifugated and the obtained solid catalyst was directly used in the next cycle. Cellulose conversion was determined by the change of cellulose weight before and after the reaction. The liquid-phase products were analyzed using a Alltech 1500 HPLC, equipped with a refractive index detector (RID). The quantification of polyols was performed using an external standard method, and the linear correlation coefficient ranges from 0.9995 to 1.0000. The yield of polyols was calculated by the equation: yield (%) = (weight of polyol in the products) / (weight of cellulose put into the reactor) × 100%. The gaseous products were checked by GC equipped with a TCD detector.

Reference

(1) Liu, J.; Sun, Z. K.; Deng, Y. H.; Zou, Y.; Li, C. Y.; Guo, X. H.; Xiong, L. Q.; Gao, Y.; Li, F. Y.; Zhao, D. Y. *Angew. Chem. Int. Ed.* **2009**, *48*, 5875-5879.

(2) a) Miyazaki, A.; Balint, I.; Aika, K.; Nakano, Y. *J. Catal.* **2001**, *204*, 364-371; b) Li, B.; Wang, D. J.; Yuan, Y. Z. H.; Takakusagi Ariga, S.; Asakura, K. *ACS Catal.* **2011**, *1*, 1521-1528; c) Liu, M.; Deng, W. P.; Zhang, Q. H.; Wang Y. L.; Wang,Y. *Chem. Commun.* **2011**, *47*, 9717-9719.

Table S1 Textural properties and Ru loading for $Ru^{2.2}/Fe_3O_4$@void@PMO-SO_3H^n

Materials	Ru Loading[a] (wt%)	BET surface area[b] ($m^2\ g^{-1}$)	Pore volume[c] ($cm^3\ g^{-1}$)	Pore size[d] (nm)	Micropore volume[e] ($cm^3\ g^{-1}$)	Micropore size[e] (nm)
$Ru^{2.2}/Fe_3O_4$@void@PMO-$SO_3H^{0.00}$	0.98	483	0.33	3.8	0.15	0.7
$Ru^{2.2}/Fe_3O_4$@void@PMO-$SO_3H^{0.08}$	1.23	363	0.31	3.8	0.17	0.7
$Ru^{2.2}/Fe_3O_4$@void@PMO-$SO_3H^{0.14}$	1.06	442	0.27	3.7	0.16	0.6
$Ru^{2.2}/Fe_3O_4$@void@PMO-$SO_3H^{0.23}$	0.87	402	0.32	3.7	0.19	0.6, 0.7
$Ru^{2.2}/Fe_3O_4$@void@PMO-$SO_3H^{0.33}$	1.31	418	0.28	3.8	0.18	0.6, 07
$Ru^{2.2}/Fe_3O_4$@void@PMO-$SO_3H^{0.43}$	0.91	422	0.30	3.6	0.17	0.6

[a] Estimated by ICP-AES; [b] the BET surface area was obtained from the adsorption branches at the relative pressure $P/P_0 = 0.2$, [c] the single point adsorption total pore volume was taken at the relative pressure of 0.96; [d] the mesopore size distribution was calculated from the adsorption branches using the Barret-Joyner-Halenda (BJH) method; and [e] microporous volume and micropore size distribution were analyzed using the Horvath-Kawazoe (H-K) method.

Table S2 Peak position and integral area from the NH_3-TPD profiles of $Ru^{2.2}/Fe_3O_4$@void@PMO-SO_3H^n

Materials	$T_{Si\text{-}OH}$ (^oC)	T_{SO3H} (^oC)	$A_{Si\text{-}OH}$	A_{SO3H}	$A_{Si\text{-}OH}/A_{SO3H}$
$Ru^{2.2}/Fe_3O_4$@void@PMO-$SO_3H^{0.00}$	-	-	-	-	-
$Ru^{2.2}/Fe_3O_4$@void@PMO-$SO_3H^{0.08}$	222	266	15	3	5.0
$Ru^{2.2}/Fe_3O_4$@void@PMO-$SO_3H^{0.14}$	245	284	39	23	1.7
$Ru^{2.2}/Fe_3O_4$@void@PMO-$SO_3H^{0.23}$	255	292	33	36	0.9
$Ru^{2.2}/Fe_3O_4$@void@PMO-$SO_3H^{0.33}$	246	291	59	88	0.7
$Ru^{2.2}/Fe_3O_4$@void@PMO-$SO_3H^{0.43}$	238	291	99	122	0.8

Table S3 NaOH titration and S analysis results

Materials	m[a] (g)	V_{NaOH} (mL)	n_{NaOH} (mol)	$C_{Si\text{-}OH+SO3H}$ (mmol g^{-1})	C_{SO3H}[b] (mmol g^{-1})	C_S (wt%)	$C_{SH+SO3H}$ (mmol g^{-1})	C_{SH}[c] (mmol g^{-1})
$Ru^{2.2}/Fe_3O_4$@void@PMO-$SO_3H^{0.00}$	0.051	0.95	0.046	0.91	0	0	0	0
$Ru^{2.2}/Fe_3O_4$@void@PMO-$SO_3H^{0.08}$	0.052	1.00	0.049	0.94	0.03	0.50	0.16	0.13
$Ru^{2.2}/Fe_3O_4$@void@PMO-$SO_3H^{0.14}$	0.052	1.25	0.061	1.19	0.28	1.34	0.42	0.14
$Ru^{2.2}/Fe_3O_4$@void@PMO-$SO_3H^{0.23}$	0.058	1.45	0.071	1.21	0.30	1.70	0.53	0.23
$Ru^{2.2}/Fe_3O_4$@void@PMO-$SO_3H^{0.33}$	0.065	1.70	0.083	1.28	0.37	1.90	0.59	0.22
$Ru^{2.2}/Fe_3O_4$@void@PMO-$SO_3H^{0.43}$	0.053	1.60	0.078	1.48	0.57	2.07	0.65	0.08

[a]mass of materials

[b]$C_{SO3H} = C_{Si\text{-}OH+SO3H} - 0.91$

[c]$C_{SH} = C_{SH+SO3H} - C_{SO3H}$

Table S4 Comparison of various catalysts used for direct conversion of cellulose to isosorbide

Entry	Materials	Cellulose amount (g)	Catalyst amount (g)	Ru content (wt%)	Reaction time (h)	Isosorbide yield[b] (%)	Productivity ($mol_{isosor}h^{-1}g_{Ru}^{-1}$)	Reference
1	Ru/C + HCl	0.20	0.02	5.0	6	49.5	0.1018	(5)
2	Ru/C + $H_4SiW_{12}O_{40}$	0.80	0.20	5.0	1	52.0	0.2567	(6)
3	Ru/C + Amberlyst-70	0.32 (BM)[a]	0.20	4.0	16	55.8	0.0087	(7)
4	Ru/$NbOPO_4$-pH2	0.24 (BM)[a]	0.20	5.0	24	13.2	0.0008	(8)
5	Ru@mNbPO	0.60	0.06	5.0	1	52.0	0.6418	(9)
6	$Ru^{2.2}/Fe_3O_4$@void@PMO-$SO_3H^{0.43}$	0.60	0.06	0.9	2	58.1	2.1900	This study

[a] The ball-milled cellulose was used.

[b] The yield of isosorbide in entries 1~5 was estimated according to the equation: yield (%) = (moles of isosorbide / moles of anhydroglucose in cellulose) × 100%.

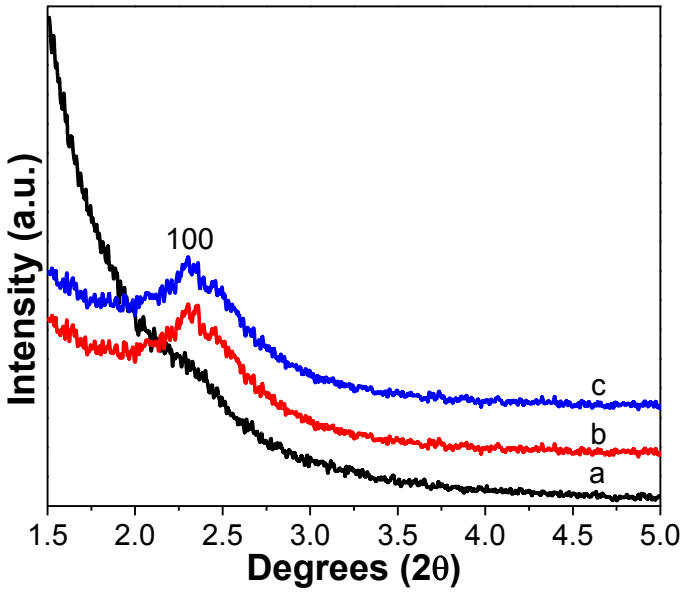

Fig. S1 XRD patterns of (a) Fe_3O_4@SiO_2@asPMO-$SH^{0.43}$, (b) Fe_3O_4@void@PMO-$SH^{0.43}$ and (c) $Ru^{2.2}$/Fe_3O_4@void@PMO-$SO_3H^{0.43}$.

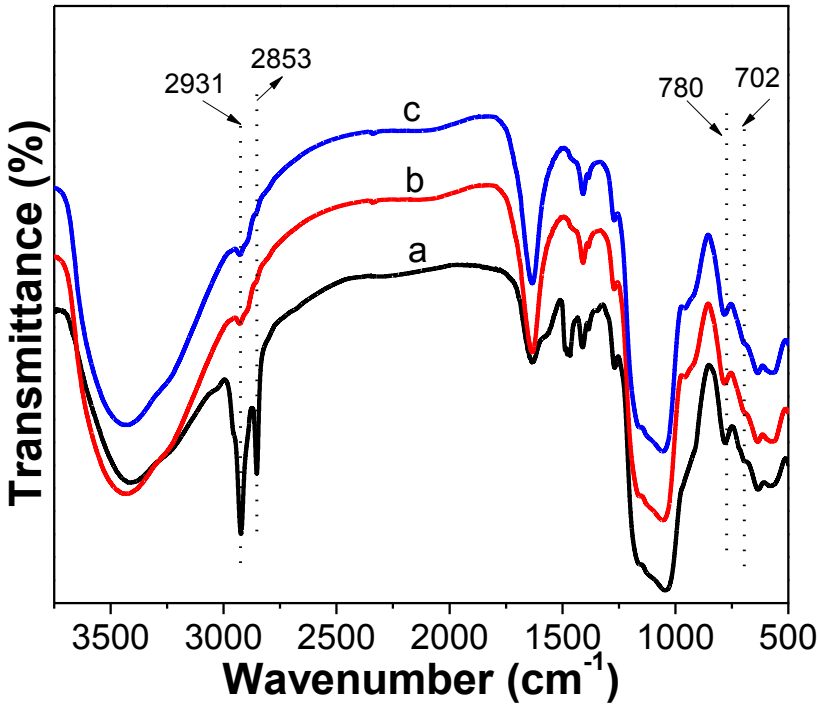

Fig. S2 FT-IR spectra of (a) Fe_3O_4@SiO_2@asPMO-$SH^{0.43}$, (b) Fe_3O_4@void@PMO-$SH^{0.43}$ and (c) $Ru^{2.2}$/Fe_3O_4@void@PMO-$SO_3H^{0.43}$.

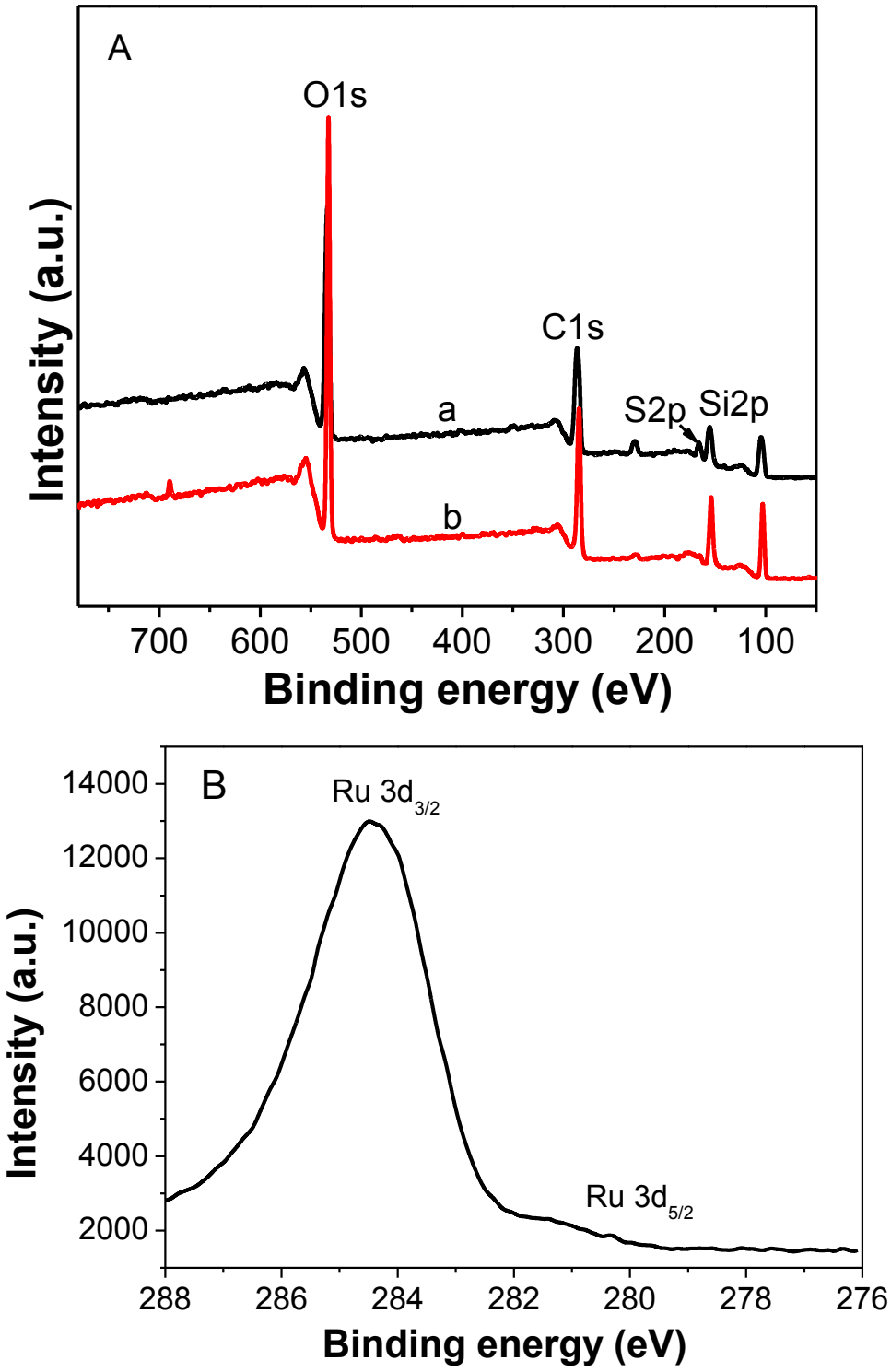

Fig. S3 (A) Survey scan of (a) Fe_3O_4@void@PMO-$SH^{0.43}$ and (b) $Ru^{2.2}$/Fe_3O_4@void@PMO-$SO_3H^{0.43}$, and (B) high-resolution Ru3d spectrum of $Ru^{2.2}$/Fe_3O_4@void@PMO-$SO_3H^{0.43}$.

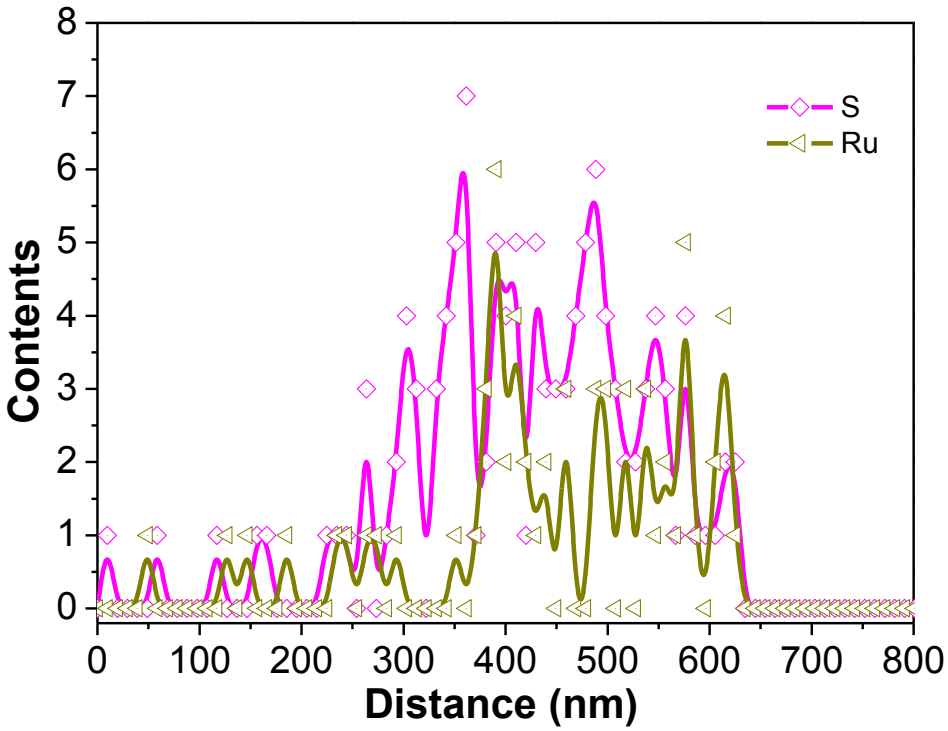

Fig. S4 Line scan profiles recorded from a single nanoreactor along the equator for S and Ru.

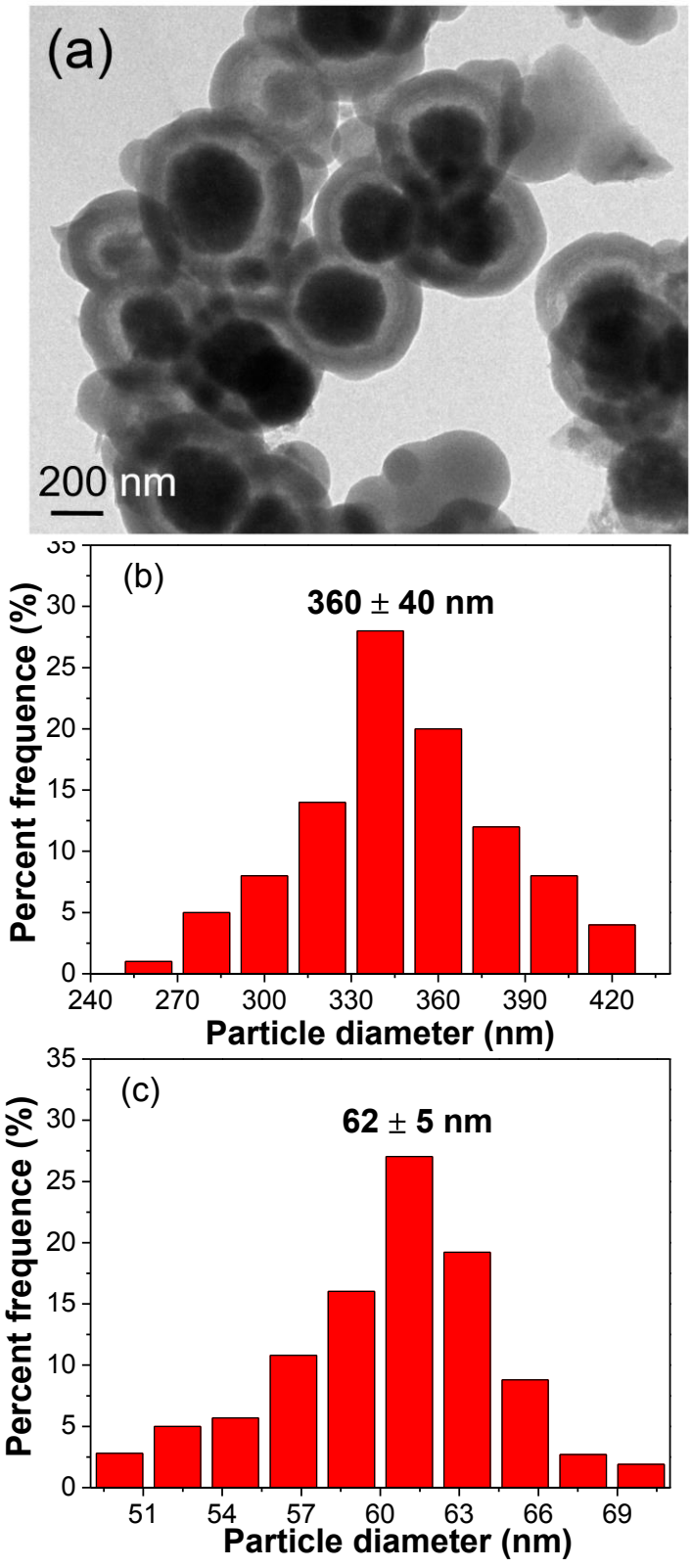

Fig. S5 TEM image (a) and the corresponding core size (b) and shell thickness (c) distribution histograms for $Ru^{2.2}/Fe_3O_4$@void@PMO-$SO_3H^{0.08}$.

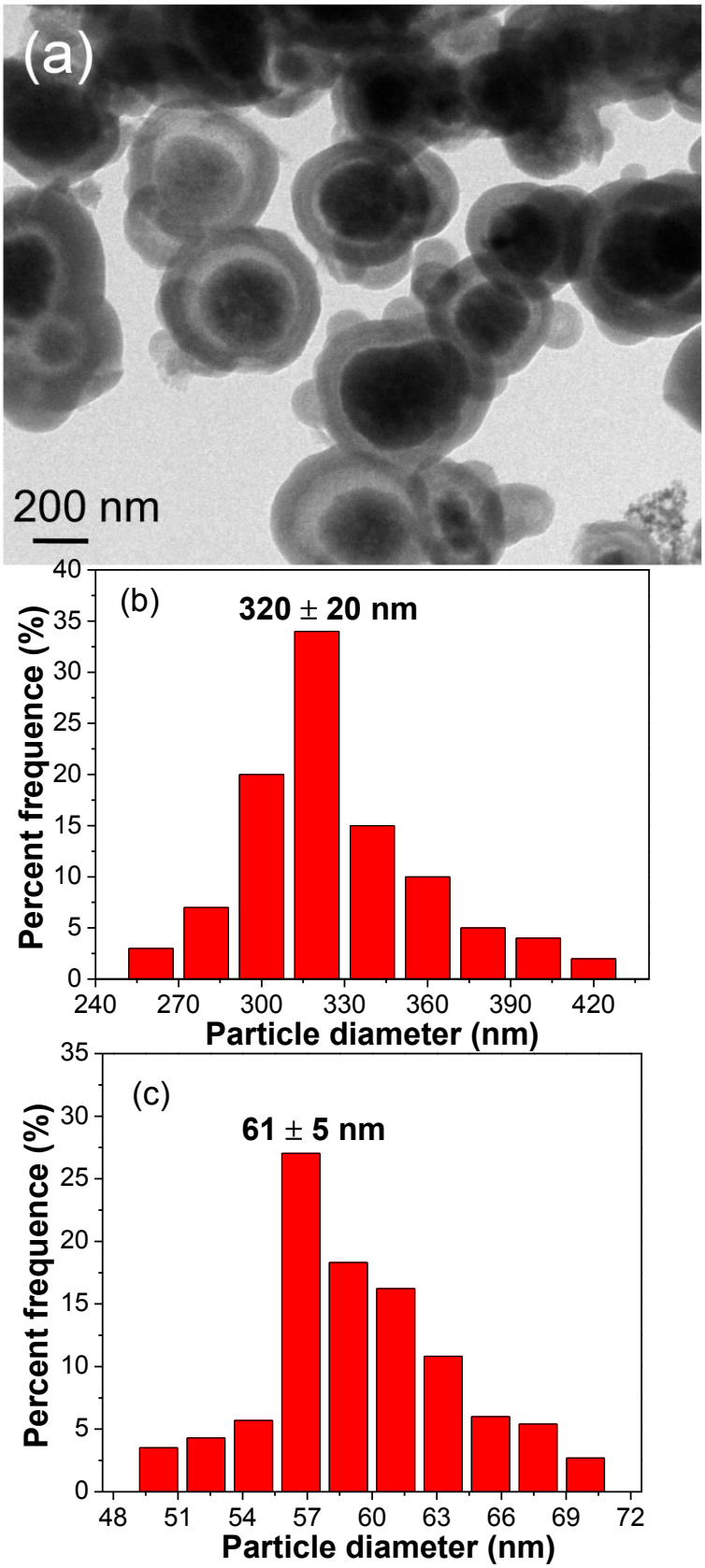

Fig. S6 TEM image (a) and the corresponding core size (b) and shell thickness (c) distribution histograms for $Ru^{2.2}/Fe_3O_4$@void@PMO-$SO_3H^{0.14}$.

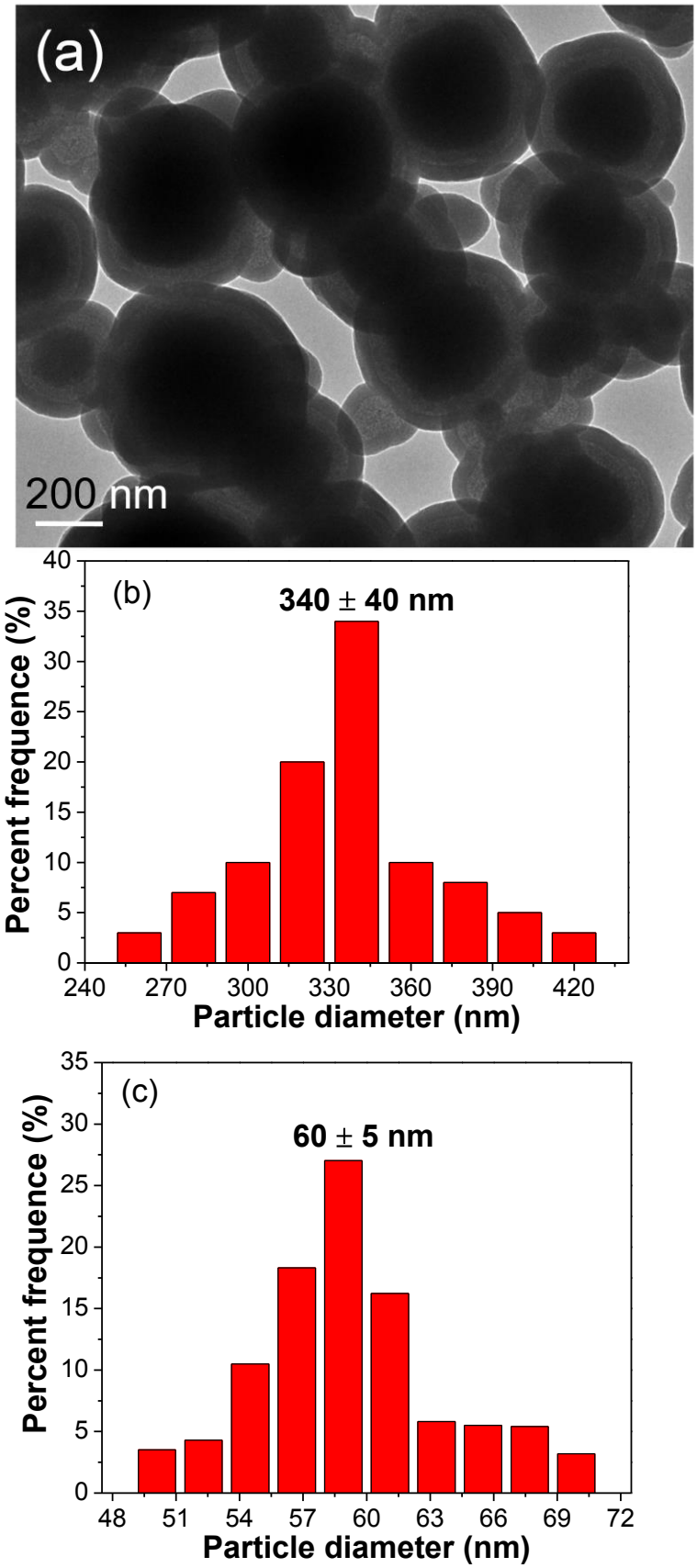

Fig. S7 TEM image (a) and the corresponding core size (b) and shell thickness (c) distribution histograms for $Ru^{2.2}/Fe_3O_4$@void@PMO-$SO_3H^{0.23}$.

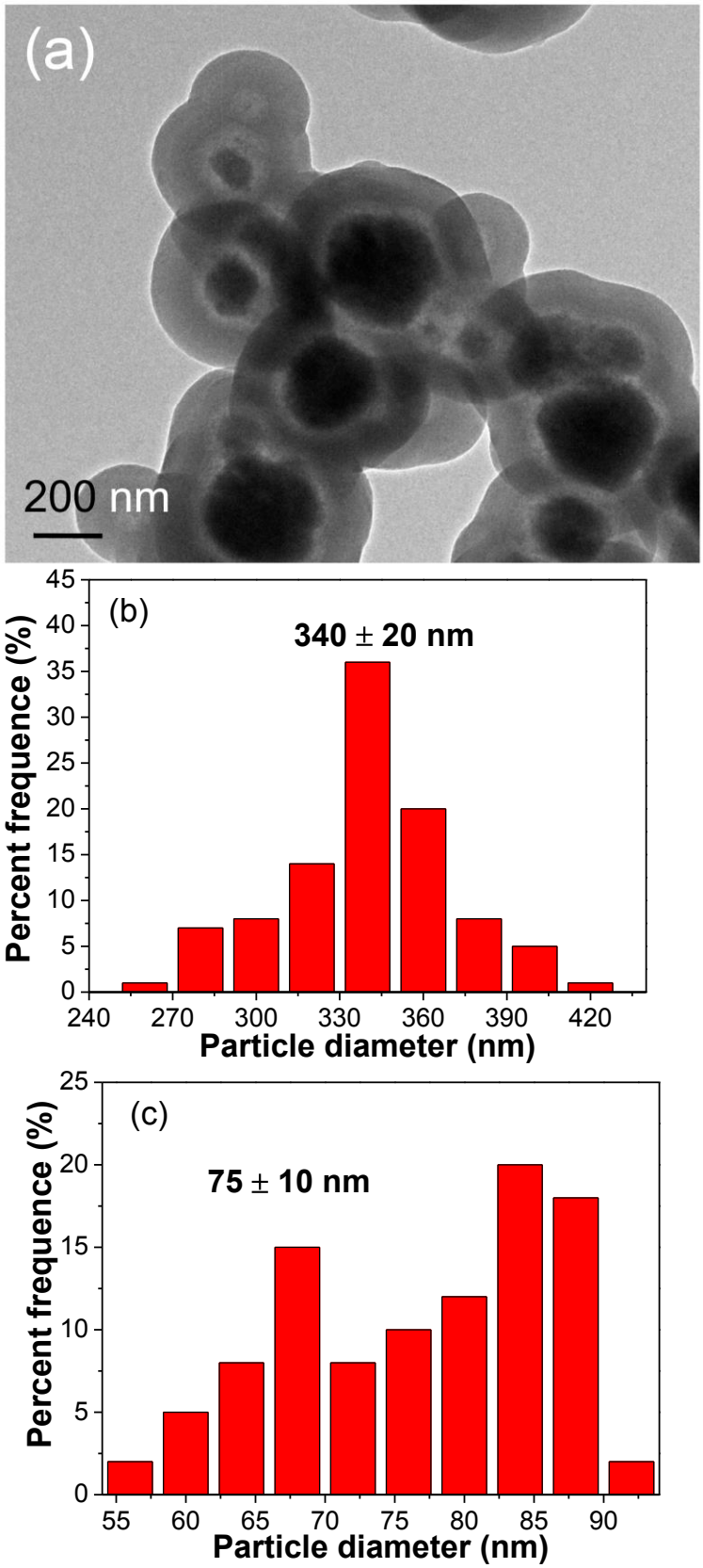

Fig. S8 TEM image (a) and the corresponding core size (b) and shell thickness (c) distribution histograms for $Ru^{2.2}/Fe_3O_4$@void@PMO-$SO_3H^{0.33}$.

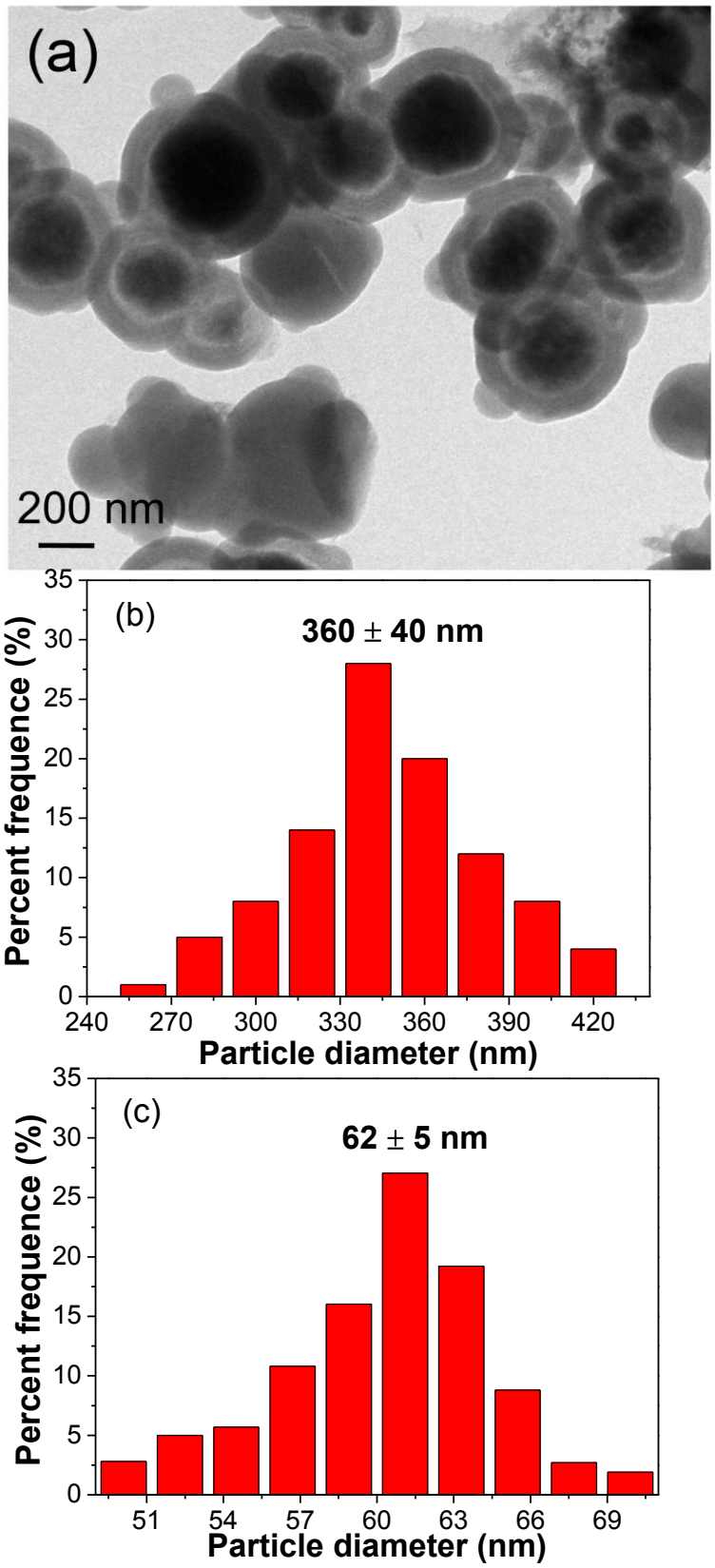

Fig. S9 TEM image (a) and the corresponding core size (b) and shell thickness (c) distribution histograms for $Ru^{2.2}/Fe_3O_4$@void@PMO-$SO_3H^{0.43}$.

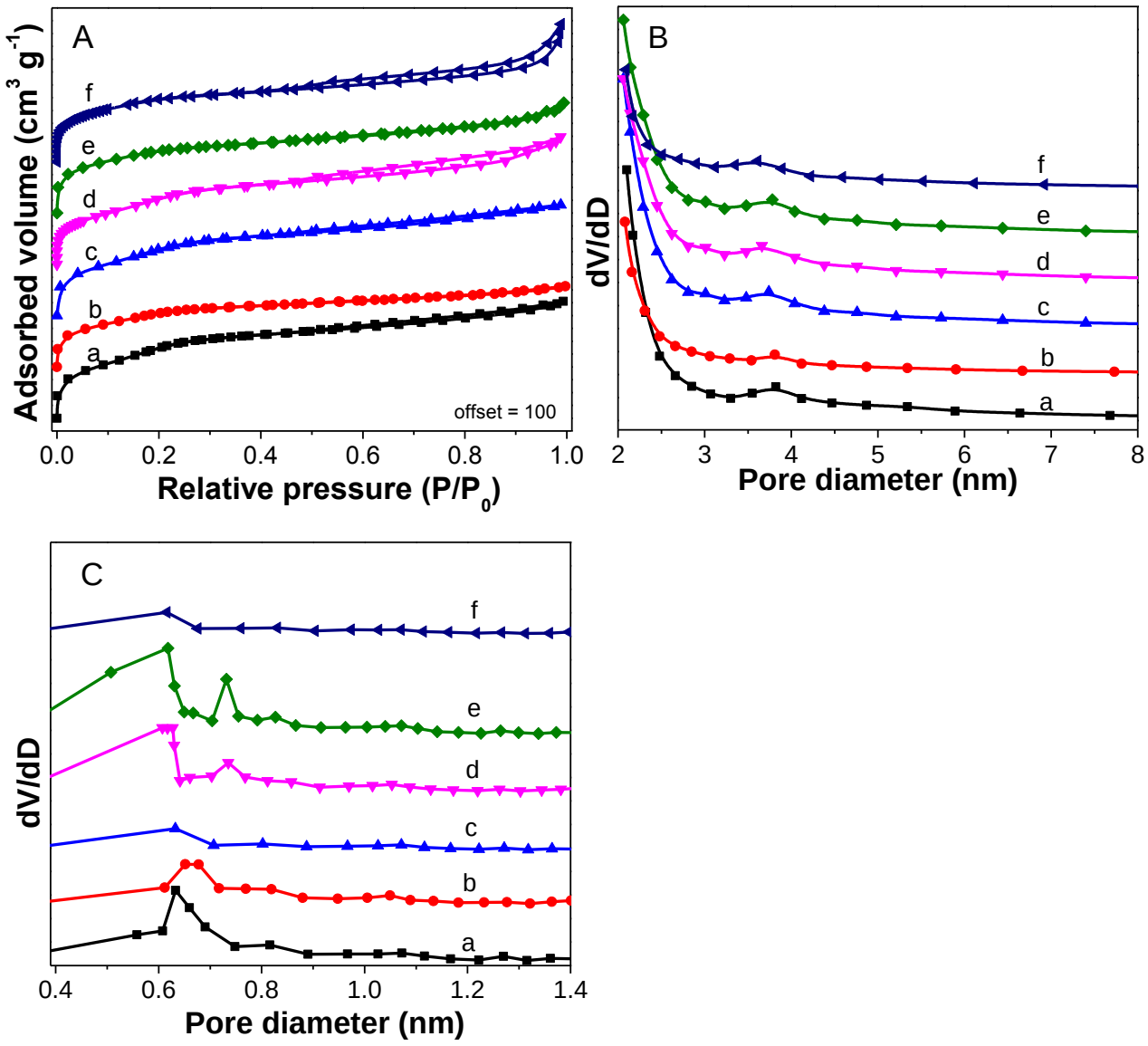

Fig. S10 N_2 adsorption/desorption isotherms (A) and the corresponding mesopore (B) and micropore size (C) distributions for (a) $Ru^{2.2}/Fe_3O_4$@void@PMO-$SO_3H^{0.00}$, (b) $Ru^{2.2}/Fe_3O_4$@void@PMO-$SO_3H^{0.08}$, (c) $Ru^{2.2}/Fe_3O_4$@void@PMO-$SO_3H^{0.14}$, (d) $Ru^{2.2}/Fe_3O_4$@void@PMO-$SO_3H^{0.23}$, (e) $Ru^{2.2}/Fe_3O_4$@void@PMO-$SO_3H^{0.33}$ and (f) $Ru^{2.2}/Fe_3O_4$@void@PMO-$SO_3H^{0.43}$.

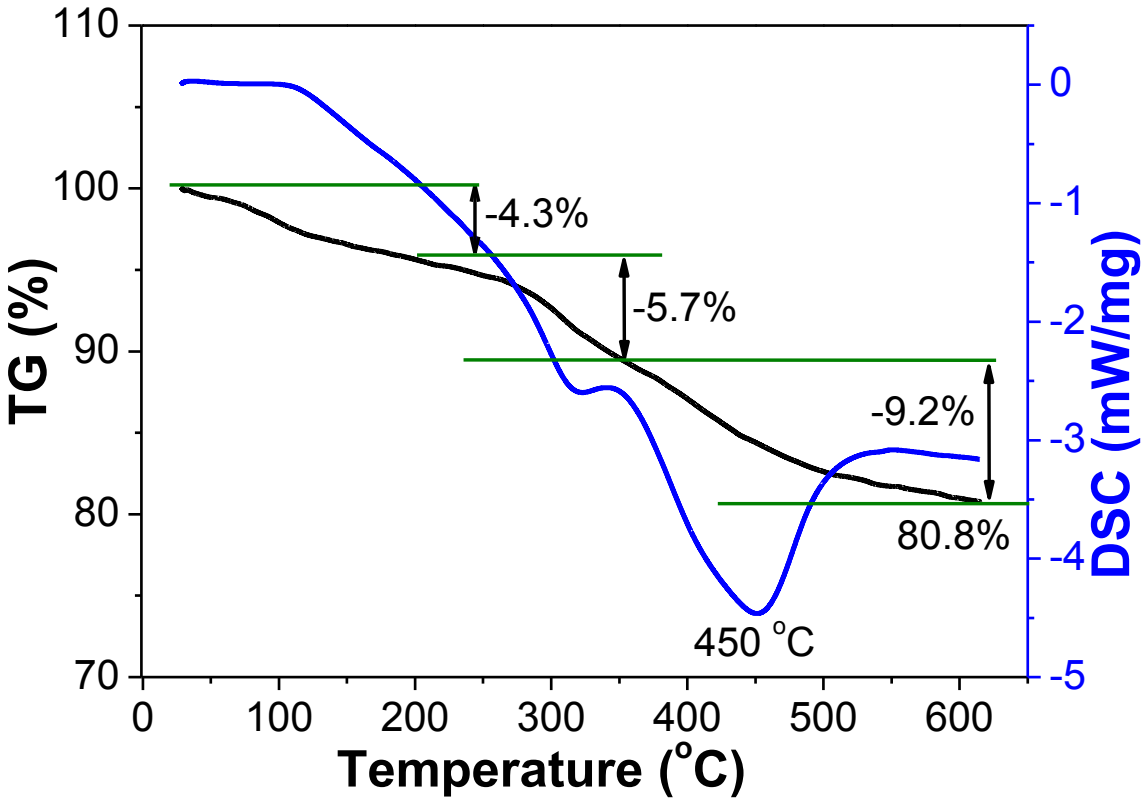

Fig. S11 TG-DSC curves for fresh $Ru^{2.2}/Fe_3O_4$@void@PMO-$SO_3H^{0.43}$.

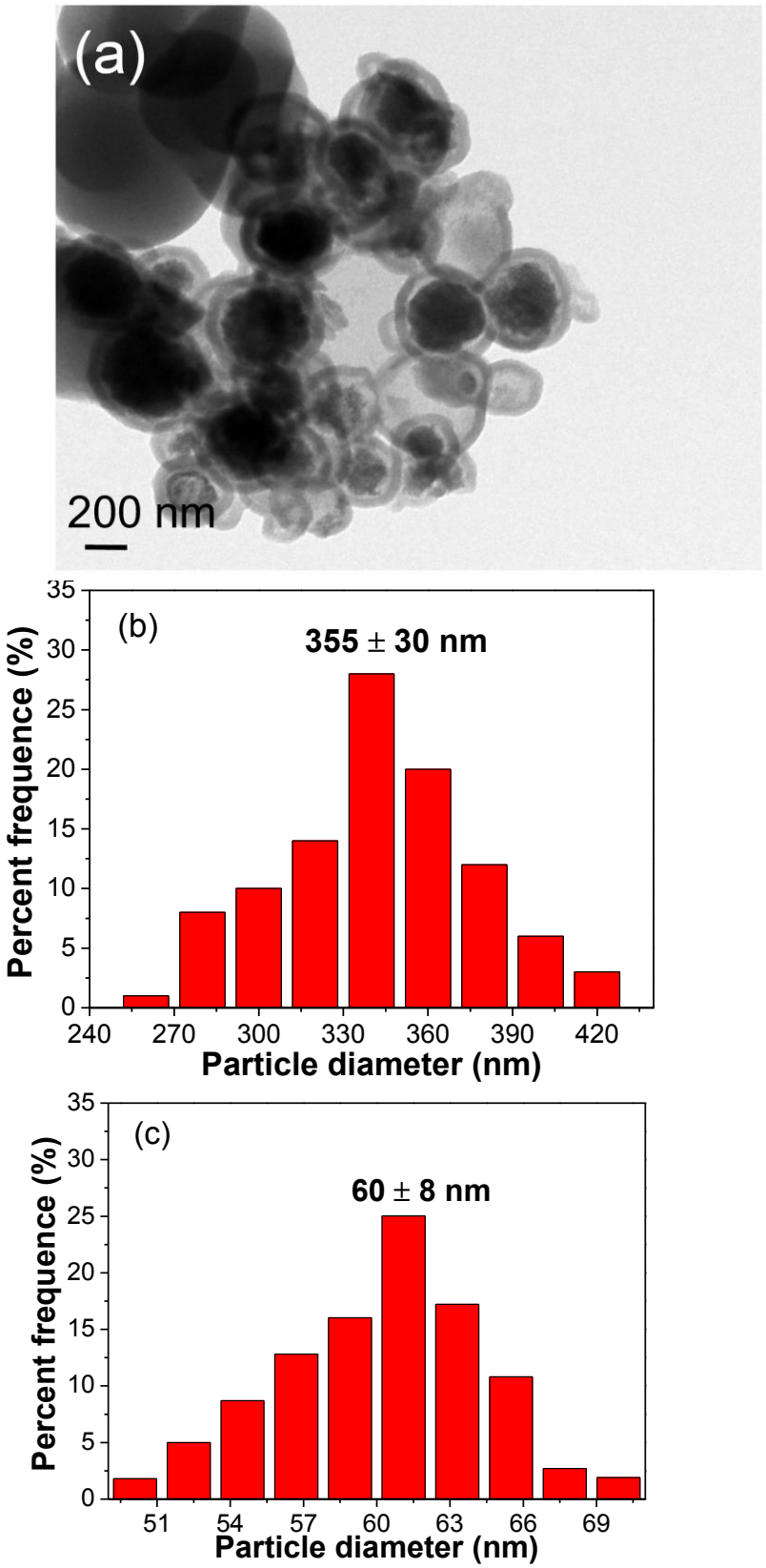

Fig. S12 TEM image (a) and the corresponding core size (b) and shell thickness (c) distribution histograms for $Ru^{2.2}/Fe_3O_4$@void@PMO-$SO_3H^{0.5}$

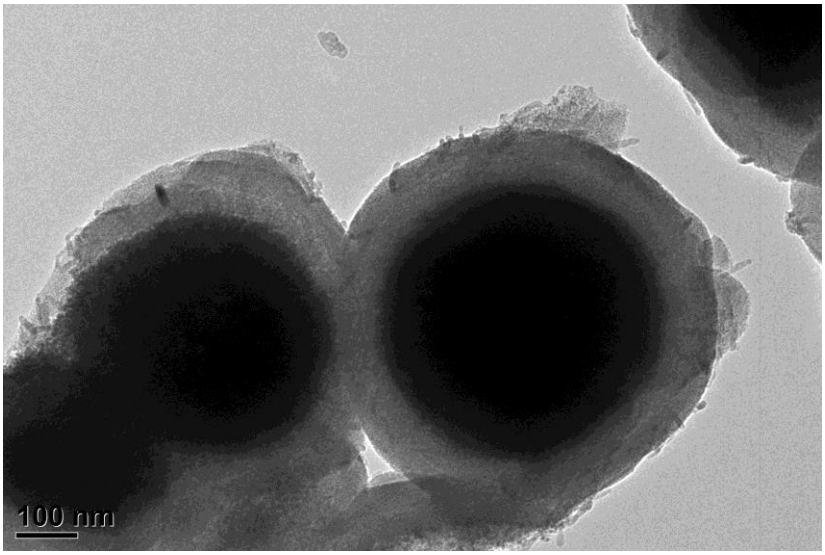

Fig. S13 TEM image of $Ru^{2.2}/Fe_3O_4@SiO_2@PMO\text{-}SO_3H^{0.43}$.

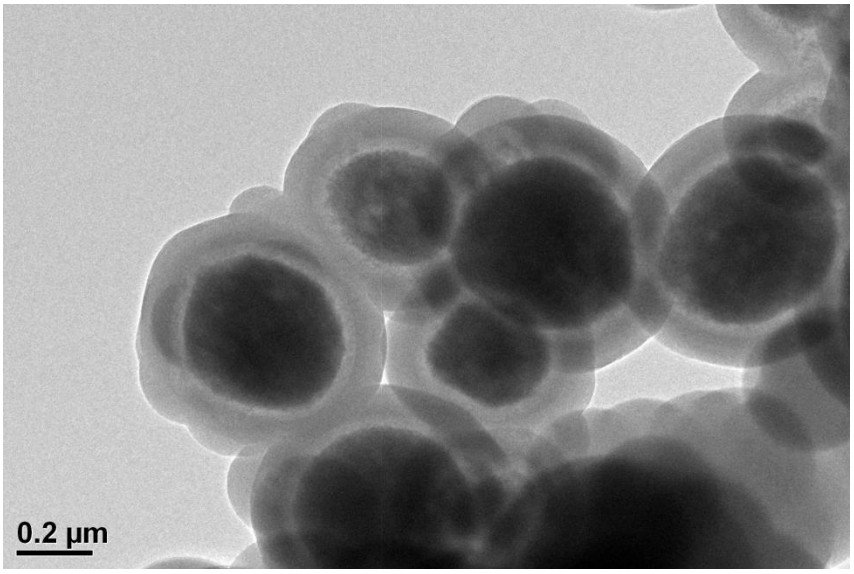

Fig. S14 TEM image of spent $Ru^{2.2}/Fe_3O_4@void@PMO\text{-}SO_3H^{0.43}$.

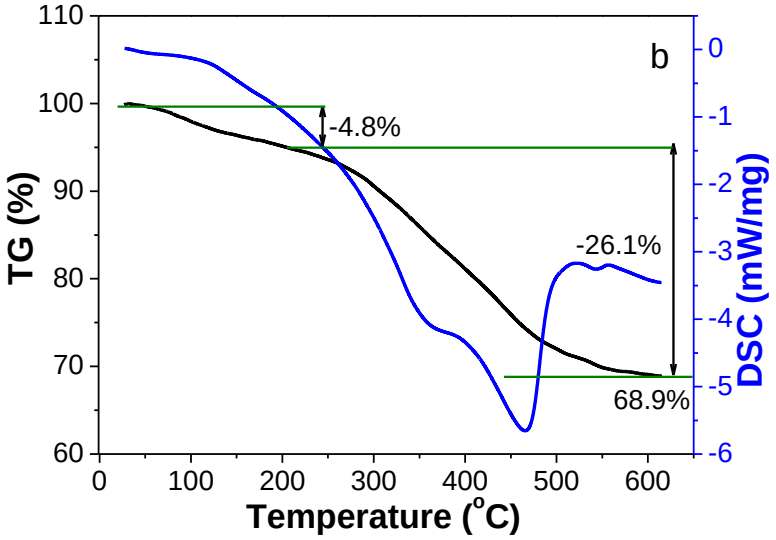

Fig. S15 TG-DSC curves for spent $Ru^{2.2}/Fe_3O_4$@void@PMO-$SO_3H^{0.43}$.